Crystal structure, magnetic, and dielectric properties of Aurivillius-type $Bi_3Fe_{0.5}Nb_{1.5}O_9$

M.W. Lufaso[a,*], W.A. Schulze[b], S.T. Misture[b], T.A. Vanderah[c]

[a]*Department of Chemistry and Physics, University of North Florida, 4567 St. Johns Bluff Road, South, Jacksonville, FL 32224, USA*
[b]*NYS College of Ceramics at Alfred University, Alfred, NY 14802, USA*
[c]*National Institute of Standards and Technology, Materials Science and Engineering Laboratory, Gaithersburg, MD 20899, USA*

Abstract

$Bi_3Fe_{0.5}Nb_{1.5}O_9$ was synthesized using conventional solid state techniques and its crystal structure was refined by the Rietveld method using neutron powder diffraction data. The oxide adopts an Aurivillius-type structure with non-centrosymmetric space group symmetry $A2_1am$ ($a = 5.47016(9)$ Å, $b = 5.43492(9)$ Å, $c = 25.4232(4)$ Å), analogous to other Aurivillius compounds that exhibit ferroelectricity. The Fe and Nb cations are disordered on the same crystallographic site. The $[(Fe,Nb)O_6]$ octahedra exhibit tilting and distortion to accommodate the bonding requirements of the Bi cations located in the perovskite double layers. Magnetic measurements indicate non-Curie–Weiss-type paramagnetic behavior from 300 to 6 K. Measurements of dielectric properties and electrical resistivity exhibited changes near 250–260 °C and are suggestive of a ferroelectric transition.
© 2007 Elsevier Inc. All rights reserved.

Keywords: Aurivillus; Polar; Crystal structure; Dielectric properties; Magnetic properties

1. Introduction

Aurivillius-type layered phases contain a regular stacking of $[Bi_2O_2]^{2+}$ slabs and perovskite-like $[A_{n-1}B_nO_{3n+1}]^{2-}$ blocks, n $[BO_6]$ octahedra in thickness [1]. Compounds exhibiting this structure-type are known which display properties suitable for applications such as non-volatile random access memory chips. Compounds which display interactions between electronic and magnetic properties are important for advanced applications such as magneto-electric (ME) devices; e.g., sensors that convert magnetic field variations into electric signals and vice versa [2]. Candidate materials include phases that crystallize in non-centrosymmetric space groups and also contain magnetically active ions. For example, dynamic ME measurements were carried out at room temperature and at 77 K on the antiferromagnetic Aurivillius-type compound $Bi_8Fe_4Ti_3O_{24}$, which exhibited a non-linear output signal [3]. The Aurivillius-type compounds $Bi_5FeTi_3O_{15}$ and $Bi_6Fe_2Ti_3O_{18}$

also display simultaneous electrical and magnetic ordering [4]. Materials with this structure-type provide important opportunities to understand the chemical and structural prerequisites for the appearance of potentially useful dielectric and magnetic properties.

The ideal structure of the archetypal $n = 2$ member of the Aurivillius-type series occurs in space group $I4/mmm$. A structural distortion is derived from the high-temperature tetragonal form by tilting of the $[BO_6]$ octahedra and displacement of B-cations in the perovskite double layers. The Aurivillius-related compounds $ABi_2M_2O_9$ ($A =$ Ca, Sr, Ba, Pb; $M =$ Nb, Ta) commonly crystallize in the non-centrosymmetric space group $A2_1am$ at ambient temperature and a number of studies have focused on their phase transitions, structures, and dielectric properties [5–9]. Solid solutions $Bi_{3-x}La_xTiNbO_9$ ($0 \leqslant x \leqslant 0.8$) were also found to crystallize in space group $A2_1am$ [10]. An intermediate phase has also been found to crystallize in space group $Amam$ for $SrBi_2Ta_2O_9$, $Sr_{0.85}Bi_{2.1}Ta_2O_9$, and $Ba_{1-x}Pb_x$ $Bi_2Nb_2O_9$ ($x = 0.375$, 0.625) [11–13]. The $Amam$ phase differs from the $A2_1am$ form in that the octahedral tilting occurs along only a single axis instead of along multiple

*Corresponding author.
E-mail address:* michael.lufaso@unf.edu (M.W. Lufaso).

axes. The high-temperature structures of these distorted members often crystallize in the archetypal tetragonal space group $I4/mmm$. The different structures exhibited by the $n = 2$ members are of particular importance because the high-symmetry phases are paraelectric, whereas the $A2_1am$ form is non-centrosymmetric and may exhibit ferroelectricity. The compound of this contribution, $Bi_3Fe_{0.5}Nb_{1.5}O_9$, is isostructural to the well-studied displacive ferroelectric Bi_3TiNbO_9. The present report describes the crystal structure, dielectric, and magnetic properties of the previously unreported Aurivillius-type phase $Bi_3Fe_{0.5}Nb_{1.5}O_9$.

2. Experimental methods

$Bi_3Fe_{0.5}Nb_{1.5}O_9$ was synthesized by the solid state method from stoichiometric amounts of Bi_2O_3 (99.999%), Nb_2O_5 (99.9985%), and Fe_2O_3 (reagent grade). Prior to each heating cycle the sample was ground with an agate mortar and pestle for 10–15 min, pelletized using a uniaxial press, and placed on same-composition sacrificial powder supported on an alumina setter plate. An initial overnight heating at 800 °C (below the m.p. of Bi_2O_3) was followed by four additional heat treatments (with soak times of 1–4 d) at 850 °C. The results of prior phase equilibria studies of the Bi_2O_3-Fe_2O_3-Nb_2O_5 system [14] indicated that $Bi_3Fe_{0.5}Nb_{1.5}O_9$ forms as a point compound, with no detectable solid solution formation, and that it begins to decompose at temperatures above 850 °C (e.g. 875 °C).

Phase purity was ascertained from X-ray powder diffraction data collected at ambient temperature using $CuK\alpha$ radiation and a Phillips[1] diffractometer equipped with incident Soller slits, a theta-compensating divergence slit and graphite monochromator, and a scintillation detector. Equilibrium was assumed when no further changes were evident in the relative intensities of the peaks. Neutron powder diffraction data were collected using the BT-1 32-detector neutron powder diffractometer at the NIST Center for Neutron Research, NBSR. The specimen was loaded in a vanadium container of length 50 mm and diameter 12.4 mm. A Cu(3 1 1) monochromator with a 90° take-off angle, $\lambda = 1.5402(2)$ Å, and in-pile collimation of 15 min of arc were used. Data were collected under ambient conditions over the range of 3–168° 2θ with a step size of 0.05°. The instrument is described at the NCNR website (http://www.ncnr.nist.gov/). Rietveld refinements were carried out using the EXPGUI interface of GSAS [15,16].

Magnetic susceptibility was measured using a Quantum Design SQUID magnetometer and a polycrystalline specimen. After cooling in the absence of an applied field, data were collected between 6 and 300 K with an applied field of

50 kG. Dielectric properties were measured using a pellet (~6.3 mm in diameter, 1.6 mm thick) pressed from single-phase powder and sintered at 850 °C for 550 h. Pellet density was approximately 60% of the theoretical density. Decomposition at higher temperatures precluded the preparation of a more highly dense specimen. Dielectric data were obtained at 1 VRMS at frequencies from 100 Hz to 1 MHz using platinum paste electrodes and a Solatron SI 1260 Impedance Analyzer. The temperature was increased from ambient to 750 °C in 5 °C steps in a Ney Centurion furnace. Resistivity was measured using a Hewlett Packard 4140B pA Meter at 1 VDC. Temperature was increased using a ramp to 1 °C/min in a Ney Centurion furnace using platinum paste electrodes.

3. Results and discussion

3.1. Crystal structure

The structure reported for Bi_3TiNbO_9 [17] was used as the starting model for $Bi_3Fe_{0.5}Nb_{1.5}O_9$. The arrangement may be described as a commensurate modulation in space group $A2_1am$. The ionic radii of Fe^{3+} and Nb^{5+} are similar, which is apparent in the octahedral cation disorder present in this phase. Attempts to independently refine the positions of Fe and Nb on the B-site resulted in an unstable refinement; therefore, the fractional coordinates and atomic displacement parameters were constrained to be equal for Fe and Nb cations. This constraint is an approximation of the structure, since it is expected that Fe^{3+} would prefer to occupy the position in the center of the octahedron, whereas the d^0 Nb^{5+} is expected to undergo an off-center displacement. A 7-term shifted Chebyschev polynomial was used to account for the background. The x fractional coordinate of Bi1 was fixed at 0.75. Lattice parameters, atomic positions, isotropic thermal parameters, pseudo-Voigt peak profile parameters, zero point, and the background function were refined. Final structural parameters and bond valence sums [18] are shown in Table 1 and selected bond lengths are shown in Table 2. The observed, calculated, and difference neutron powder diffraction

Table 1
Fractional coordinates and bond valence sums for $Bi_3Fe_{0.5}Nb_{1.5}O_9$

	Occ.	x	y	z	U_i/U_e*100	BVS (v.u.)
Bi1	1	0.75	0.7387(6)	0	2.26(7)	2.91
Bi2	1	0.7557(7)	0.7692(4)	0.20007(6)	1.71(4)	2.82
Fe	0.25	0.8054(5)	0.7500(4)	0.58807(6)	0.76 (3)	3.16
Nb	0.75	0.8054(5)	0.7500(4)	0.58807(6)	0.76 (3)	4.77
O1	1	0.8473(9)	0.3213(7)	0	1.60(9)	1.90
O2	1	0.8147(7)	0.6935(4)	0.65931(8)	1.43(7)	1.64
O3	1	0.0291(7)	−0.0051(5)	0.24993(10)	1.01(5)	2.30
O4	1	0.0383(8)	0.9679(5)	0.06685(9)	1.11(5)	1.90
O5	1	0.1236(7)	0.9440(5)	0.41496(10)	1.07(6)	1.86

Space group $A2_1am$, $a = 5.47016(9)$ Å, $b = 5.43492(9)$ Å, $c = 25.4232(4)$ Å, volume $= 755.83(2)$ Å^3. Refinement fitting details: R_{wp} (%) 5.13, R_p (%) 4.29, $R(F^2)$ (%) 4.10, $\chi^2 = 1.52$.

patterns are shown in Fig. 1. The inset to Fig. 1 shows the splitting of the 315/135 reflections near 56° 2θ, indicative of orthorhombic symmetry. Structural refinements were attempted in space group *Amam*, corresponding to the intermediate phase, but the refinements were inferior to those in space group $A2_1am$. Although not investigated in this study, a sequence of phase transitions $A2_1am$-*Amam*-$I4/mmm$ may occur for $Bi_3Fe_{0.5}Nb_{1.5}O_9$, as found for $SrBi_2Ta_2O_9$, $Sr_{0.85}Bi_{2.1}Ta_2O_9$, and $Ba_{1-x}Pb_xBi_2Nb_2O_9$ ($x = 0.375, 0.625$) [11,12,19].

The crystal structure of $Bi_3Fe_{0.5}Nb_{1.5}O_9$ is shown in Fig. 2. The Fe and Nb atoms occupy the $[MO_6]$ octahedra in the perovskite blocks, with the O–(Fe/Nb)–O chains along the *c*-axis interrupted by $[Bi_2O_2]^{2+}$ layers. The octahedra exhibit significant distortion, with bond distances ranging from 1.838(3) to 2.284(2) Å, and with *trans*-O1–*M*–O2, O5–*M*–O4, and O4–*M*–O5 bond angles of 172.6(6)°, 160.5(3)°, and 160.3(3)°, respectively. The bond valence sums (Table 1) suggest the presence of slight residual bond strain within the $[MO_6]$ octahedra; i.e., overbonding (compression) about Fe^{3+} (BVS = 3.16 v.u.) and underbonding (tension) about Nb^{5+} (BVS = 4.77 v.u.). Part of the discrepancy is correlated with the position

Table 2
Selected interatomic distances (Å)

Bi1–O1	2.330(5)	Fe/Nb–O1	2.284(2)
Bi1–O1	2.227(5)	Fe/Nb–O2	1.838(3)
Bi1–O4	2.632(4)	Fe/Nb–O4	2.065(4)
Bi1–O4 (×2)	2.602(3)	Fe/Nb–O4	1.957(4)
Bi1–O4	2.632(4)	Fe/Nb–O5	2.036(3)
Bi1–O5	2.477(3)	Fe/Nb–O5	1.939(3)
Bi2–O2	2.549(3)	Bi2–O3	2.313(4)
Bi2–O2	2.633(4)	Bi2–O3	2.465(4)
Bi2–O3	2.188(4)	Bi2–O3	2.283(3)

constraints used on the octahedral cations. The bond distances given in Table 2 are typical based on ionic radii and the bond valence sums are in reasonable agreement with the formal oxidation states [20,21].

The crystal structures of Bi_3TiNbO_9 and $Bi_3Fe_{0.5}Nb_{1.5}O_9$ are very similar. In addition to the similar connectivity of the atoms, the octahedral B-cations undergo an off-center distortion of approximately 0.3 Å from the symmetric position. This was calculated by defining a plane through four oxygen atoms (O4 and O5) in the octahedral layer approximately in the *ab* plane and calculating the distance between the plane and the B-cation. There are minor differences in the *M*–O–*M* bond angles. The Nb/Ti–O–Nb/Ti bond angles in the octahedral layer of the crystal structure are 148.8(6)° and 153.8(4)° in the *ab* plane and 148.1(1)° along the *c*-axis for Bi_3TiNbO_9 [17]. By comparison, in $Bi_3Fe_{0.5}Nb_{1.5}O_9$ the Nb/Fe–O–Nb/Fe bond angles are 146.9(3)° and 151.7(3)° in the *ab* plane and 157.3(6)° along the *c*-axis. The *M*–O–*M* bond angles in the *ab* plane are slightly more linear for Bi_3TiNbO_9 than $Bi_3Fe_{0.5}Nb_{1.5}O_9$; however, the *M*–O–*M* bond angle along the *c*-axis is somewhat more linear for $Bi_3Fe_{0.5}Nb_{1.5}O_9$ than for Bi_3TiNbO_9. Additionally, the lattice parameter ratios $c/a = 4.65$ and $c/b = 4.68$ for $Bi_3Fe_{0.5}Nb_{1.5}O_9$ are larger than $c/a = 4.61$ and $c/b = 4.65$ for Bi_3TiNbO_9. Assuming the $[Bi_2O_2]^{2+}$ layer does not significantly contribute to the differences, the larger lattice parameter ratio and more linear *M*–O–*M* bond angle along the *c*-axis for $Bi_3Fe_{0.5}Nb_{1.5}O_9$ are consistent with a larger contribution of octahedral tilting along the *c*-axis and less along the *a*- and *b*-axes, relative to the octahedral tilting in Bi_3TiNbO_9.

The cooperative tilting of the octahedra about two axes is illustrated in Fig. 2. The tilting accommodates the Bi1 cations located in the cavity formed by the corner-sharing
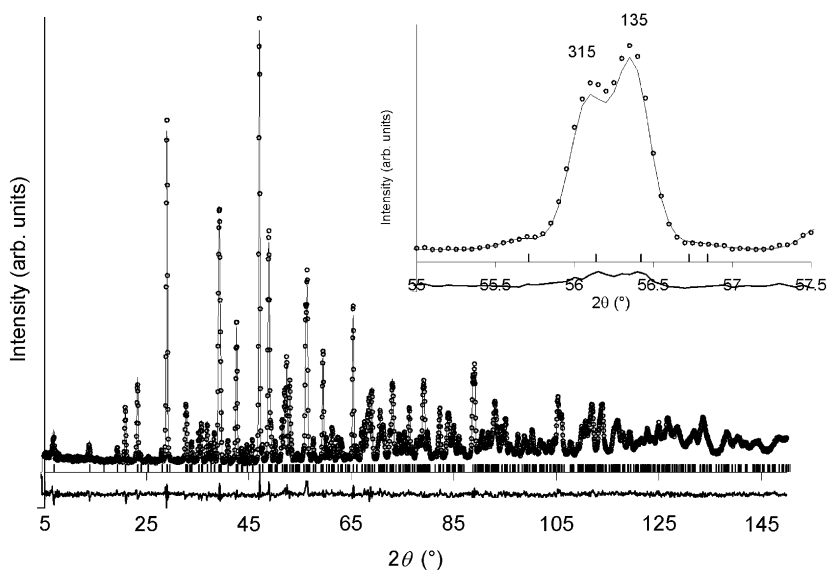

Fig. 1. Observed and calculated neutron diffraction pattern for $Bi_3Fe_{0.5}Nb_{1.5}O_9$. The difference reflection is shown at the bottom. Tick marks indicate allowed reflections. The inset shows the splitting of the (3 1 5)/(1 3 5) reflections near 56° 2θ, which is indicative of orthorhombic symmetry.
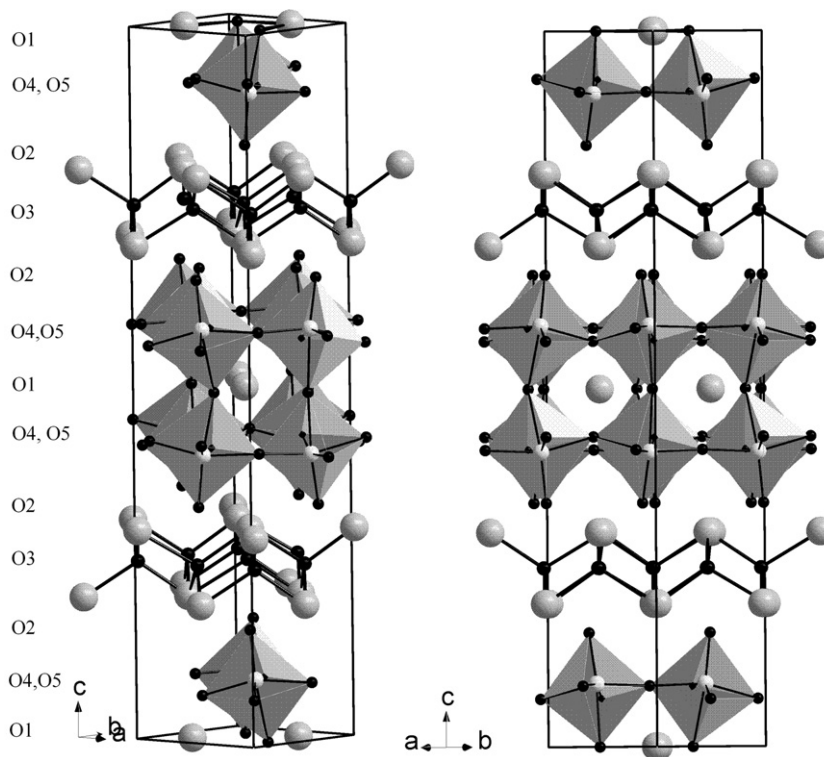
Fig. 2. Crystal structure of $Bi_3Fe_{0.5}Nb_{1.5}O_9$ viewed approximately along the 1,−1,0 (left) and 1,1,0 (right). Large gray spheres represent Bi, small black spheres are O, and gray octahedra contain disordered Nb and Fe.

octahedra, and the bond valence sum of Bi1 is reasonable at 2.82 v.u. The atomic displacements along the *a*-axis relative to the corresponding positions in the parent tetragonal ($I4/mmm$) structure cause ferroelectric spontaneous polarization. In contrast, polarization from atomic displacements along the *b*- and *c*-axes is cancelled by the presence of glide and mirror planes, respectively, and does not contribute to the total polarization. An estimation of the total ferroelectric spontaneous polarization and relative contributions of each ion to the total spontaneous polarization was calculated for $Sr_{0.8}Bi_{2.2}Ta_2O_9$ and $SrBi_2Ta_2O_9$ by comparing the structure in the polar space group to the high symmetry structure in space group $I4/mmm$ [22]. An approximation of the spontaneous polarization may be calculated by considering the contribution of each ion to the total spontaneous polarization by fixing the *x* fractional coordinate position of the Bi1 atom at $\frac{3}{4}$, and using the expression

$$P_s = \sum_i (f \times m_i \times \Delta x_i \times Q_i e)/V,$$

where *f* is the fractional site occupancy, m_i is the site multiplicity, Δx_i is the atomic displacement along the *a*-axis from the high symmetry position in the $I4/mmm$ structure, $Q_i e$ is the ionic charge for the ion, and *V* is the unit cell volume. The results are illustrated schematically in Fig. 3. The calculated polarization of $Bi_3Fe_{0.5}Nb_{1.5}O_9$ is 31 μC/cm² and is comparable to, but slightly higher than, the isostructural compounds $Sr_{0.8}Bi_{2.2}Ta_2O_9$ and $SrBi_2Ta_2O_9$
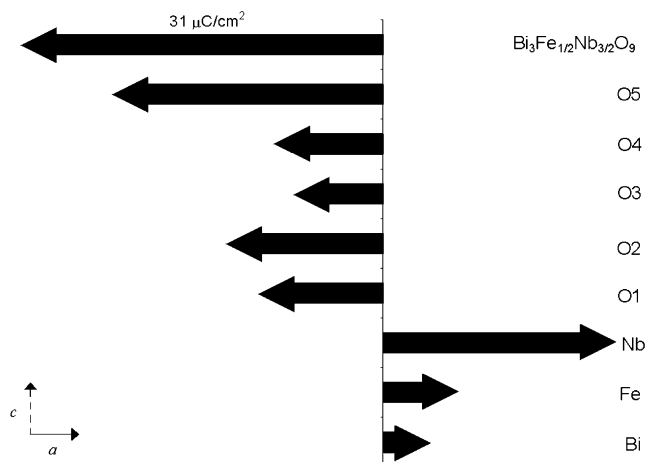

Fig. 3. Schematic drawing of the contribution of each ion to the total ferroelectric spontaneous polarization of $Bi_3Fe_{0.5}Nb_{1.5}O_9$. The position of the Bi1 site on the *a*-axis was fixed at 0.75.

with calculated values of 20 and 18 μC/cm², respectively [22]. The calculation tends to overestimate the spontaneous polarization, for example, $Sr_{0.8}Bi_{2.2}Ta_2O_9$ has a reported spontaneous polarization of ∼7 μC/cm² [22]. Although the large atomic displacements of Bi2 in the $[Bi_2O_2]^{2+}$ layers and of O5 in the $(Fe,Nb)O_6$ octahedra give a large contributions to the spontaneous polarization used in the calculation, it has been shown that the off-center displacement of Bi^{3+} is the underlying cause for the ferroelectric

distortion [23]. If O5 had been chosen to fix the origin, then Bi1 would show the dominant contribution to the polarization. The same convention, fixing Bi1, was used to enable a comparison with previously reported values. It is noteworthy that this calculation tends to overestimate the spontaneous polarization, so a smaller experimentally measured polarization is anticipated compared with the predicted value.

3.2. Magnetic properties

The magnetic and inverse magnetic susceptibility vs. temperature for $Bi_3Fe_{0.5}Nb_{1.5}O_9$ are shown in Fig. 4. The compound is paramagnetic with no indication of a magnetic phase transition. The Curie–Weiss law is not obeyed in the temperature range examined, as can be seen from the poor linear fit between 100 and 300 K. Paramagnetism is common for Aurivillius-type compounds; for example, $Bi_2Sr_2Nb_2MnO_{12-\delta}$ exhibited paramagnetic behavior when the Mn was located on one crystallographic site [24], and $Bi_2Sr_{1.4}La_{0.6}Nb_2MnO_{12}$ was reported to exhibit spin-glass behavior [25]. Extrapolation of the inverse magnetic susceptibility vs. temperature results in a negative intercept, which suggests antiferromagnetic interactions are present. The disorder on the B-type cation sublattice in $Bi_3Fe_{0.5}Nb_{1.5}O_9$ may also contribute to the non-Curie–Weiss-type behavior, since potential magnetic coupling between iron cations may be disrupted. Further studies are necessary to elucidate the magnetic interactions among the Fe cations; however, the present results reveal no magnetic phase transition between 6 and 300 K.
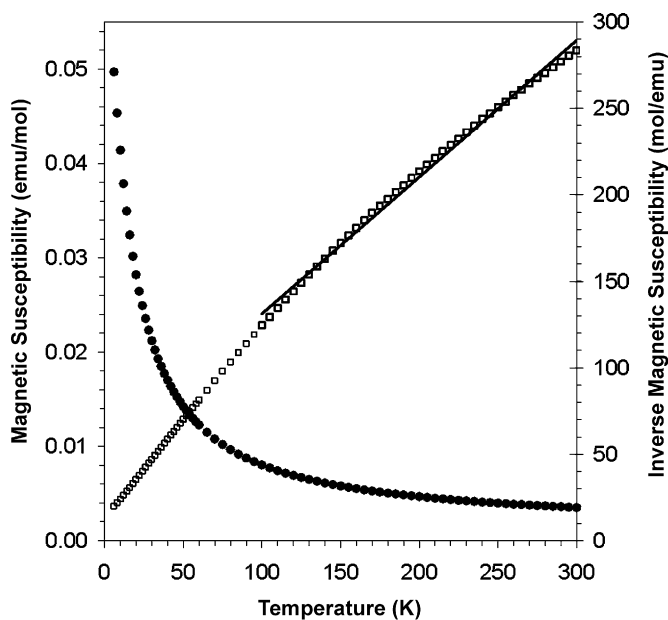
3.3. Dielectric properties

Despite the low density of the specimens, both the relative permittivity and resistivity were measured. The temperature dependence of the relative permittivity is shown in Fig. 5 (top) and the resistivity vs. inverse temperature is shown in Fig. 5 (bottom). At 1, 10, and 100 kHz, a decrease in the relative permittivity is observed between 250 and 260 °C. At 1 MHz, the decrease in relative permittivity is no longer evident, and there is an unusually large shift in the permittivity with frequency. Given the high conductivity at high temperature, the broad shift in permittivity with frequency is likely a result of conductivity-dominated interfacial polarization. A similar frequency dependence of the upturns in relative permittivity has also been observed in other oxides where the sample becomes predominantly conductive [14,26]. There is a clear change in the resistivity near 250 °C, also suggesting a phase transition occurs. The apparent activation energy for dc conduction decreases from 1.38 to 0.67 eV in the region of the
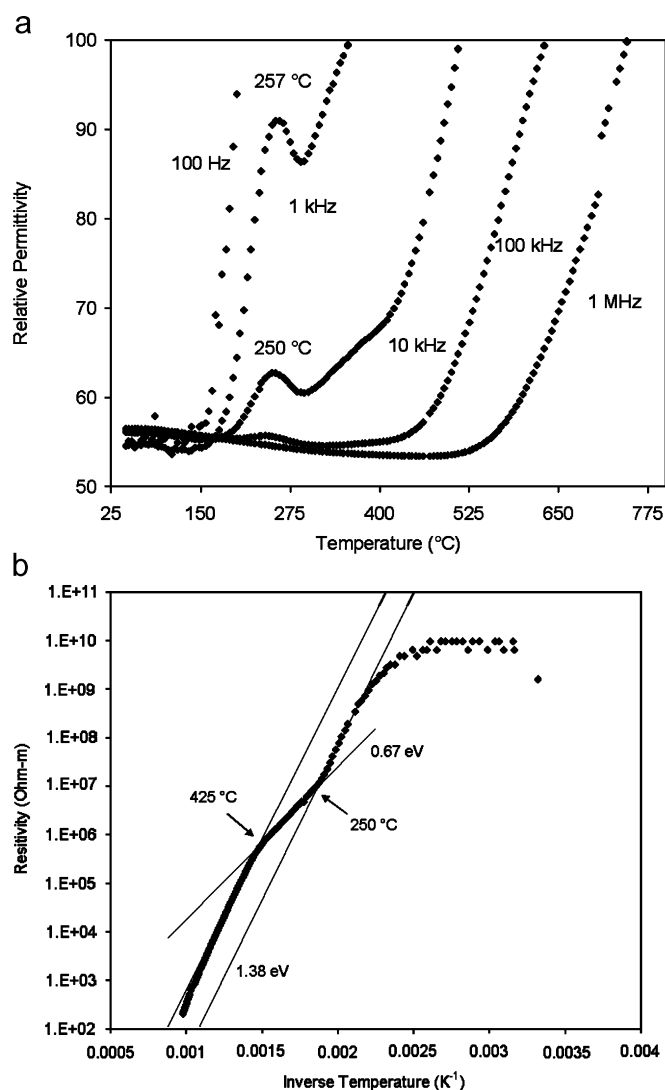

Fig. 4. Temperature dependence of the zero-field-cooled magnetic susceptibility of $Bi_3Fe_{0.5}Nb_{1.5}O_9$ at an applied field of 50 kG. The magnetic behavior deviates from the Curie–Weiss linear fit shown between 100 and 300 K.

Fig. 5. Temperature dependence of the relative permittivity (top) and conductivity (bottom) for $Bi_3Fe_{0.5}Nb_{1.5}O_9$.

dielectric anomaly near 250 °C. The activation energy for conduction then returns to 1.38 eV at 425 °C and remains constant to 700 °C. Such changes in slope are consistent with a ferroelectric phase transition. It is noteworthy that the transition temperature of $\sim$255 °C for $Bi_3Fe_{0.5}Nb_{1.5}O_9$ is significantly lower than the transition temperature of $\sim$950 °C reported for Bi_3TiNbO_9 [27].

4. Conclusion

$Bi_3Fe_{0.5}Nb_{1.5}O_9$, a new Aurivillius-type compound, has been synthesized and its structure refined using neutron powder diffraction data. $Bi_3Fe_{0.5}Nb_{1.5}O_9$ crystallizes in the non-centrosymmetric space group $A2_1am$, analogous to other isostructural ferroelectric Aurivillius-type phases. No magnetic phase transitions were observed between 6 and 300 K, and the compound exhibits paramagnetic behavior that deviates from Curie–Weiss-type behavior. The change in resistivity and the presence of a peak in the relative permittivity near 250–260 °C (523–533 K) indicates the existence of a ferroelectric phase transition.

Acknowledgment

References

[1] B. Aurivillius, Ark. Kemi 1 (1949) 463.
[2] L. Fuentes, M. Garcia, J. Matutes-Aquino, D. Rios-Jara, J. Alloys Compds. 369 (2004) 10.
[3] A. Srinivas, D.W. Kim, K.S. Hong, S.V. Suryanarayana, Mater. Res. Bull. 39 (2004) 55.
[4] A. Srinivas, S.V. Suryanarayana, G.S. Kumar, M.M. Kumar, J. Phys. Condens. Matter 11 (1999) 3335.
[5] C.A.P. De Araujo, J.D. Cuchiaro, L.D. Mcmillan, M.C. Scott, J.F. Scott, Nature 374 (1995) 627.
[6] Ismunandar, B.A. Hunter, B.J. Kennedy, Solid State Ionics 112 (1998) 281.
[7] R. Macquart, B.J. Kennedy, Y. Shimakawa, J. Solid State Chem. 160 (2001) 174.
[8] S.M. Blake, M.J. Falconer, M. McCreedy, P. Lightfoot, J. Mater. Chem. 7 (1997) 1609.
[9] B.J. Kennedy, B.A. Hunter, Chem. Mater. 13 (2001) 4612.
[10] G. Nalini, G.N. Subbanna, T.N. Guru Row, Mater. Chem. Phys. 82 (2003) 663.
[11] C.H. Hervoches, J.T.S. Irvine, P. Lightfoot, Phys. Rev. B 64 (2001) 100102(R).
[12] R. Macquart, B.J. Kennedy, B.A. Hunter, C.J. Howard, Y. Shimakawa, Integr. Ferroelectr. 44 (2002) 101.
[13] R. Macquart, B.J. Kennedy, T. Kamiyama, F. Izumi, J. Phys. Condens. Matter 16 (2004) 5443.
[14] M.W. Lufaso, T.A. Vanderah, I.M. Pazos, I. Levin, R.S. Roth, J.C. Nino, V. Provenzano, P.K. Schenck, J. Solid State Chem. 179 (2006) 3874.
[15] A.C. Larson, R.B. von Dreele, General Structure Analysis System (GSAS), Los Alamos National Laboratories, 1990.
[16] B.H. Toby, J. Appl. Crystallogr. 34 (2001) 210.
[17] J.G. Thompson, A.D. Rae, R.L. Withers, D.C. Craig, Acta Cryst. B 47 (1991) 174.
[18] N.E. Brese, M. O'Keeffe, Acta Cryst. B 47 (1991) 192, with updated R_0 parameters, ⟨http://www.ccp14.ac.uk/ccp/web-mirrors/i_d_brown/⟩.
[19] R. Macquart, B.J. Kennedy, T. Kamiyama, F. Izumi, J. Phys. Condens. Matter 16 (2004) 5443.
[20] R.D. Shannon, Acta Cryst. A 32 (1976) 751.
[21] I.D. Brown, Chem. Soc. Rev. 7 (1978) 359.
[22] Y. Shimakawa, Y. Kubo, Y. Nakagawa, T. Kamiyama, H. Asano, F. Izumi, Appl. Phys. Lett. 74 (1999) 1904 and references therein.
[23] A.D. Rae, J.G. Thompson, R.L. Withers, Acta Cryst. B 48 (1992) 418.
[24] W.J. Yu, Y.I. Kim, D.H. Ha, J.H. Lee, Y.K. Park, S. Seong, N.H. Hur, Solid State Commun. 111 (1999) 705.
[25] E.E. McCabe, C. Greaves, J. Mater. Chem. 15 (2005) 177.
[26] T.A. Vanderah, T. Siegrist, M.W. Lufaso, M.C. Yeager, R.S. Roth, J.C. Nino, S. Yates, Eur. J. Inorg. Chem. (2006) 4908.
[27] X. Zhang, P. Gu, S.B. Desu, Phys. Status Solidi (a) 160 (1997) 35.